Comparative density-functional LCAO and plane-wave calculations of LaMnO$_3$ surfaces

R. A. Evarestov,[1,2] E. A. Kotomin,[1,3] Yu. A. Mastrikov,[1] D. Gryaznov,[1] E. Heifets,[4] and J. Maier[1]

[1]*Max Planck Institute for Solid State Research, Heisenbergstraße 1, D-70569 Stuttgart, Germany*
[2]*Department of Quantum Chemistry, St. Petersburg University, 198504 St. Peterhof, Russia*
[3]*Institute for Solid State Physics, University of Latvia, Kengaraga Str. 8, Riga LV-1063, Latvia*
[4]*Materials and Physics Simulation Center, Beckman Institute, California Institute of Technology,*
MS 139-74 Pasadena, California 91125, USA

We compare two approaches to the atomic, electronic, and magnetic structures of LaMnO$_3$ bulk and the (001), (110) surfaces—hybrid B3PW with optimized LCAO basis set (CRYSTAL-2003 code) and GGA-PW91 with plane-wave basis set (VASP 4.6 code). Combining our calculations with those available in the literature, we demonstrate that combination of nonlocal exchange and correlation used in hybrid functionals allows to reproduce the experimental magnetic coupling constants J_{ab} and J_c as well as the optical gap. Surface calculations performed by both methods using slab models show that the antiferromagnetic (AF) and ferromagnetic (FM) (001) surfaces have lower surface energies than the FM (110) surface. Both the (001) and (110) surfaces reveal considerable atomic relaxations, up to the fourth plane from the surface, which reduce the surface energy by about a factor of 2, being typically one order of magnitude larger than the energy difference between different magnetic structures. The calculated (Mulliken and Bader) effective atomic charges and the electron density maps indicate a considerable reduction of the Mn and O atom ionicity on the surface.

PACS number(s): 68.35.Bs, 68.35.Md, 68.47.Gh

I. INTRODUCTION

Understanding and control of surface properties of pure and doped LaMnO$_3$ is important for applications in fuel cells,[1] magnetoresistive devices, and spintronics.[2] However, manganite surface properties are studied very poorly, especially theoretically. There are two reports of local spin-density functional approximation (LSDA) calculations on CaMnO$_3$ and La$_{0.5}$Ca$_{0.5}$MnO$_3$ (001) surfaces[3] and of two self-interaction corrections (SIC)-LSD calculations on solid solution La$_{1-x}$Sr$_x$MnO$_3$ (001) surfaces.[2] These density functional theory (DFT) studies focused mostly on low-temperature magnetic properties and neglected surface relaxation as well as surface energy calculations. On the other hand, there exists a series of LaMnO$_3$ bulk electronic structure calculations, using a number of the first-principles methods—e.g., unrestricted Hartree-Fock (UHF) LCAO,[4–6] LDA+U,[7] and relativistic full-potential generalized gradient approximation (GGA) LAPW.[8] These studies mostly deal with the magnetic properties of LaMnO$_3$, in particular the energetics of the ferromagnetic (FM) and antiferromagnetic (AF) phases. The experiments show that below 750 K the cubic phase of LaMnO$_3$ with a lattice constant of a_0=3.95 Å is transformed into the orthorhombic phase (four formula units per unit cell). Below T_N=140 K the A-type AF configuration (AAF) is the lowest in energy. This corresponds to the ferromagnetic coupling in the basal ab (xy) plane combined with antiferromagnetic coupling in the c (z) direction in the *Pbnm* setting. Also FM, GAF and CAF magnetic states exist: FM corresponds to a fully ferromagnetic material, in GAF all the spins are antiferromagnetically coupled to their nearest neighbors, and in CAF cell the spins are antiferromagnetically coupled in the basal plane and ferromagnetically between the planes (along the c axis). However, only in a few papers was the attempt made to compare

calculations with the experimental magnetic coupling constants (see below).

Recently, we performed a series of LaMnO$_3$ calculations with a focus on the (110) surface (using both classical shell model[9–11] and HF[12,13]) and the polar (001) surface[13,14] (HF and DFT plane-wave calculations). In these studies, we focused on the surface energy calculations for stoichiometric and nonstoichiometric slabs with different terminations and analyzed the electronic density redistribution near the surface. However, in these studies the surface relaxation was taken into account only in the shell model (110) calculations[9–11] and recent VASP calculations for the (001) surface.[14] In recent years, *hybrid* DFT-HF Hamiltonians combined with the LCAO basis set attracted considerable attention due to their ability to reproduce very well the electronic and magnetic structure and, in particular, the optical gap of the ABO_3 perovskites.[15] The DFT approach overestimates delocalization of the electron density due to nonexact cancellation of the electron self-interaction. This effect is important for well-localized Mn atom electrons in LaMnO$_3$ and is partly taken into account in SIC-LDA approach. As an alternative, the hybrid functionals are used, which take into account an explicit orbital dependence of the energy through nonlocal part of the exchange (see more in the review article in Ref. 16).

In this paper, we compare critically the potential of the two *ab initio* DFT approaches—hybrid B3PW LCAO and GGA-PW—to calculate basic properties of LaMnO$_3$. Section II deals with computational details and bulk properties. Surface properties are discussed and compared in Sec. III, while in Sec. IV conclusions are presented.

II. COMPUTATIONAL DETAILS AND BULK PROPERTIES

In our simulations of LaMnO$_3$ bulk crystals and its surfaces we used two different formalisms of density functional

theory as implemented into CRYSTAL-2003[17] and VASP 4.6[18] computer codes. The former presents the crystalline orbitals in a form of linear combination of atomic orbitals (LCAO). The latter uses the crystalline orbital expansion in the plane waves (PW's). In LCAO the atomic orbitals themselves are expanded into a set of localized atom-centered Gaussian-type orbitals (GTO's). In DFT LCAO calculations we applied Becke three-parameter hybrid functional (B3PW),[19] which uses in the exchange part the mixture of the Fock (20%) and Becke's (80%) exchange, whereas in the correlation part Perdew-Wang (PWGGA) nonlocal correlation functional are employed.[20] Our previous experience[21] shows that this functional gives the best description of the atomic and electronic structures, as well as elastic properties of several ABO_3 perovskite materials. In some cases, for a comparison the B3LYP (Ref. 15) hybrid functional was also used (the exchange part is the same as in B3PW functional and the correlation is the Lee-Yang-Parr nonlocal functional[22]).

In the PW calculations Perdew-Wang-91 GGA nonlocal functional was used both for exchange and correlation, since PW calculations with hybrid functional are impossible at the moment. We tried preliminarily[14] three types of the projector augmented-wave pseudopotentials for the inner electrons— La, Mn, O; La, Mn_{pv}, O_s; and La, Mn_{pv}, O, where the lower index pv means that p states are treated as valence states and s stands for soft pseudopotentials with reduced cutoff energy and/or reduced number of electrons. As a result, we used here the second set of pseudopotentials suggesting a good compromise between computational time and accuracy. We used the Monkhorst-Pack scheme for $\boldsymbol{k}$-point mesh generation, which was typically 4 4 4 (if not otherwise stated). The calculated cohesive energy of 30.6 eV/unit cell is in perfect agreement with the experimental estimate of 30.3 eV. The optimized lattice parameters and atomic coordinates in the orthorhombic cell are close to the experimental values.[23] Energetically the most favorable is the AAF configuration, in agreement with experimental data. Hereafter, we call this method GGA-PW.

The choice of PW basis is simple as it is defined only by the cutoff energy. In our calculations it was chosen to be 600 eV, if not otherwise stated. More difficult is the problem of basis set (BS) choice in the LCAO calculations. It is well known that standard GTO's used in molecules do not provide a suitable BS for solids, due to diffuse orbitals causing linear dependences between atomic orbitals (AO's) centered on different atoms. For many atoms the GTO BS is available on the CRYSTAL code homepage site;[24] in some cases, an additional basis optimization is necessary.

In this paper, such BS optimization was performed for $LaMnO_3$ using the procedure applied earlier[21] to similar CRYSTAL calculations for titanates with the perovskite structure. In present calculations, B3PW total energy was used for optimizing exponents of GTO's and the coefficients in their contractions to AO's. $LaMnO_3$ in a cubic FM phase with the experimental (high-temperature cubic phase) lattice constant of 3.95 Å was considered as the reference. For the oxygen atoms, an all-electron (AE) $8\text{-}411(1d)G$ basis was taken from previous perovskite calculations.[21] This basis set includes eight Gaussian-type functions contracted into a single basis function describing $1s$ core electrons and three groups

of basis functions consisting of four, one, and one Gaussians for a description of the $2s$ and $2p$ valence electrons. The oxygen basis includes also a separate polarized d-type Gaussian orbital.

We replaced Mn and La ions core electrons with Hay-Wadt small-core (HWSC) pseudopotentials.[25] This significantly reduces computational efforts for simulations, especially in the slab modeling of surfaces. It will be shown below that it does not essentially affect the results for bulk $LaMnO_3$, in comparison with those obtained in an all-electron treatment of La and Mn ions. We developed the BS of $411(311d)G$ for Mn ion and $411(1d)G$ for the La ion. In order to perform Gaussian exponent optimization, we used a small computer code written by one of us (E.H.). This code serves as an external optimization driver, which makes inputs for CRYSTAL code from a template, reads the total energy from the CRYSTAL output, and performs necessary computations, in order to determine the next set of input parameters. The code uses final differences to compute the total energy derivatives over AO parameters (exponents and expansion coefficients). The optimization is performed by means of the conjugated gradient technique.

The BS optimization was made in two steps. As a first step, we optimized basis functions for Mn^{2+} and La^{2+} ions. We specially chose ionic charges smaller than formal charges of Mn^{3+} and La^{3+} ions in $LaMnO_3$ crystal, because the calculated Mulliken charges of these ions are usually much smaller than the formal charges.[4–6,12] The electron shells of Mn^{2+} and La^{2+} ions are open: the Mn^{2+} ion has five more electrons with α spin than with β spin, and the La^{2+} ion has one more electron with α spin than with β spin. Therefore, at the first step we applied a spin-polarized self-consistent procedure to calculate the electronic structure and the total energies of these ions. At the second step, we minimized the total energy of $LaMnO_3$ crystal, varying the exponents of the most diffuse Gaussian functions on Mn and La ions, and keeping frozen all parameters of the contracted inner atomic basis functions on Mn and La ions (contracted functions contain more than one Gaussian) and parameters of all basis functions of oxygen atoms.

In previous $LaMnO_3$ bulk calculations using HF (Refs. 4, 5, and 12) and hybrid HF-DFT (Ref. 6) LCAO four different BS's were used (noted in Table I as BS1–BS4), whereas the above-described BS optimized for $LaMnO_3$ is denoted as BS5. In BS1–BS5 the AE basis was used on oxygen atoms but only BS4 and BS5 include polarization d-GTO. Similar GTO's for core and $2sp$ valence states were used in BS1–BS5; they differ, however, in the outermost exponents describing virtual states: in BS1, $3sp$ and $4sp$ outer GTO's were optimized in $LaMnO_3$ UHF calculations[5] or taken from UHF calculations of $CaMnO_3$ (Ref. 26) (BS2, BS3) or MnO (Ref. 27) (BS4) with BS optimization.

For the La^{3+} ion, the AE BS1 (Ref. 5) was optimized in UHF calculations as $8\text{-}76333(63d)$ $1s$, $2sp$, $3sp$, $4sp$, $5sp$ $(3d,4d)$, respectively, adding polarized $6sp$ orbitals with a single exponent. When using the BS2 basis, La was treated as a bare La^{3+} ion represented by the effective Hay-Wadt large-core (HWLC) pseudopotential.[25] In BS3 the La atom core was represented by a small core ($5s$, $5p$ core electrons are considered as valence electrons) pseudopotential of Dolg

TABLE I. The B3PW LCAO calculated total energies (in a.u.), Mn atom magnetic moments μ (in μ_B), and charges Q (in e) for a primitive cubic unit cell of LaMnO$_3$. The results were obtained with an experimental lattice constant of 3.95 Å. The energies for nonspin and $S_z=1, 2$ solutions are given with respect to the energy of the $S_z=0$ state.

	E ($S_z=0$)	Q_{La}	Q_{Mn}	Q_O	ΔE (NM)	Q_{La}	Q_{Mn}	Q_O	ΔE ($S_z=1$)	Q_{La}	Q_{Mn}	Q_O	μ	ΔE ($S_z=2$)	Q_{La}	Q_{Mn}	Q_O	μ
BS1[a]	-9600.58	3.16	1.65	-1.60	-0.015 09	3.16	1.63	-1.6	-0.074 13	3.16	1.71	-1.62	1.87	-0.131 27	3.16	1.85	-1.67	3.96
BS2[b]	-1378.21	—	1.56	-1.52	-0.015 66	—	1.54	-1.51	-0.074 11	—	1.63	-1.54	1.86	-0.129 31	—	1.78	-1.59	3.96
BS3[c]	-1408.44	2.47	1.56	-1.34	-0.017 11	2.46	1.54	-1.33	-0.076 25	2.47	1.62	-1.36	1.87	-0.133 21	2.46	1.76	-1.41	3.96
BS4[d]	-361.16	2.28	1.85	-1.37	-0.017 95	2.26	1.84	-1.37	-0.080 57	2.27	1.91	-1.39	1.90	-0.144 11	2.26	2.00	-1.42	3.97
BS5[e]	-361.19	2.60	1.85	-1.48	-0.016 71	2.60	1.84	-1.48	-0.081 48	2.60	1.91	-1.50	1.90	-0.146 87	2.60	2.00	-1.53	4.00
PW	-154.08	1.93	1.71	-1.22	0.000 01	1.93	1.71	-1.22	-0.2045	1.93	1.78	-1.24	2.00	-0.037 92	1.94	1.90	-1.29	4.00

[a]Reference 5.
[b]Reference 4.
[c]Reference 6.
[d]Reference 12.
[e]Present study.

et al.[28] In BS4 the HWSC pseudopotential was used to replace core electrons and the orbital exponents were taken from La$_2$CuO$_4$ calculations.[29]

Mn atoms were also represented differently in BS1–BS5. In particular, in BS1, BS2, and BS3 the same AE basis was taken: 86-411(41d) with two d-orbital exponents, optimized for CaMnO$_3$ and modifying the outermost d exponent to 0.259 (BS1, BS2) or 0.249 (BS3). In BS4 the Mn atom basis 311(31d) was taken from the CRYSTAL web site[24] which corresponds to the HWSC pseudopotential substituting core electrons.

In order to check how the results depend on the basis choice, we performed B3LYP and B3PW LCAO calculations for the cubic LaMnO$_3$ with one formula unit per primitive cell with the experimental lattice constant of 3.95 Å. The relative smallness of the various total energy differences (FM-AF, bulk-slab) requires a high numerical accuracy in the lattice and Brillouin zone summations. Following (Ref. 6) the cutoff threshold parameters of CRYSTAL for Coulomb and exchange integrals evaluation (ITOL1–ITOL5) have been set to 7, 7, 7, 7, and 14, respectively. The integration over the Brillouin zone (BZ) has been carried out on the Monkhorst-Pack grid of shrinking factor 8 (its increase up to 16 gave only a small change in the total energy per unit cell). The self-consistent procedure was considered as converged when the total energy in the two successive steps differs by less than 10^{-6} a.u.

In Table I we compare the total energies for the cubic primitive unit cell of five atoms obtained in non-spin-polarized B3PW calculations (NM) and spin-polarized B3PW calculations with different magnetic ordering of four d electrons on the Mn^{3+} ion: total spin projection $S_z=2$ (four α electrons occupy t_{2g} and e_g levels), $S_z=1$ (three α electrons and one β electron occupy the t_{2g} level), and $S_z=0$ (two α electrons and two β electrons occupy the t_{2g} level). To model these situations in the CRYSTAL code, we used options allowing us to fix the initial magnetic ordering on the Mn atom. The calculated self-consistently spin density on the Mn atom is given also in Table I. The total energy per primitive cell is highest for $S_z=0$ (second column of Table I). Since the number of electrons per cell depends on the basis used, the absolute values of these energies are also quite different. In the next columns of Table I the relative energies per unit cell and the magnetic moments of Mn atom are given for different spin projections (the energy for $S_z=0$ is taken for zero). The basis optimization for the same number of electrons per unit cell results in a lower energy for the same spin projection (compare BS4 and BS5 in Table I). The important result is that the *order* of relative energies for different magnetic configurations is the same for all BS and even absolute values of energy differences are close. Table I shows that the Mulliken atomic charges remain the same for different magnetic orderings, provided the BS is fixed. At the same time, their absolute values show the BS dependence for the same spin projection value. It is seen also that for Mn^{3+} ion in a crystal the Hund rule holds and the lowest energy corresponds to the maximal spin projection.

The last line of Table I presents the results of the VASP calculations.[14] The GGA-PW potential for exchange-correlation and the projector augmented-wave (PAW)

TABLE II. The energy (in meV per unit cell) of the different magnetic phases for orthorhombic LaMnO$_3$ [for the experimental structure (Ref. 30)]. The energy of the FM configuration is taken as zero energy. Magnetic moments μ on Mn atom in μ_B, magnetic coupling constants J_{ab} and J_c in meV. Experimental data: μ=3.87 for AAF (Ref. 36), J_c=−1.2, J_{ab}=1.6 (Ref. 31).

Method/basis set	AAF	μ	GAF	μ	CAF	μ	J_c	J_{ab}
UHF(BS1)[a]	−4.8	—	55.6	—	—	—	−0.15	0.94
B3LYP(BS1)[b]	−33.0	3.80	112.0	3.72	120.0	3.73	−0.64	2.07
UHF(BS2)[c]	−8.0	—	48.0	—	56.0	—	−0.25	0.88
B3LYP(BS2)[b]	−33.0	3.78	84.0	3.71	101.0	3.71	−0.78	1.70
UHF(BS3)[d]	−5.2	3.96	51.2	—	55.9	—	−0.15	0.88
Fock-50(BS3)[d]	−12.2	3.89	89.22	—	93.64	—	−0.26	1.52
B3LYP(BS3)[d]	−32.2	3.80	114.0	—	121.5	—	−0.62	2.09
B3LYP(BS4)[b]	−32.0	3.81	103.0	3.73	117.0	3.76	−0.72	1.97
B3LYP(BS5)[b]	−30.0	3.82	106.0	3.74	117.0	3.77	−0.64	1.98
B3PW(BS5)[b]	−19.0	3.86	153.0	3.75	152.0	3.79	−0.28	2.50
GGA-PW91(BS5)[b]	−40.0	3.71	248.0	3.58	234.0	3.64	−0.83	4.08
GGA-PW[b]	−59.0	3.55	189.0	3.35	224.0	3.46	−1.47	3.69
LAPW[e]	−72.0	—	96.0	—	136.0	—	−1.75	2.38
LMTO[f]	−62.0	3.46	243.0	3.21	—	—	−1.94	4.76
FLMTO(GGA)[g]	−98.8	—	142.8	—	167.2	—	−1.92	3.19
LDA+U[h]	−34.0	—	170.0	—	—	—	−1.06	2.66

[a]Reference 5.
[b]Present work. PW91 stands for the standard exchange–correlation functional by Perdew and Wang (Ref. 20).
[c]Reference 4.
[d]Reference 6.
[e]Reference 32.
[f]Reference 34.
[g]Reference 33.
[h]Reference 35.

pseudopotentials for core electrons (42 electrons) were used here with the semicore La 5s 5p and Mn 3p states treated as valence states. The topological (Bader) charges are also given for all the magnetic orderings. It is seen that the relative energies of different magnetic orderings reveal the same sign in PW DFT and LCAO calculations (the lowest energy corresponds to S_z=2). The Bader atomic charges (compared with Mulliken charges) are much smaller and also show a weak dependence on the magnetic ordering.

To study the magnetic ordering in LaMnO$_3$, the so-called *broken symmetry approach* was adopted.[6] It allows one to deduce the magnitude of the magnetic coupling data making spin-polarized calculations for different magnetic orderings of transition metal atoms. LaMnO$_3$ is stabilized at moderate temperatures in the *orthorhombic structure* comprising four formula units, space group D_{2h}^{16} (in *Pbnm* and *Pnma* settings the largest orthorhombic lattice translation vector is directed along the z or y axis, respectively; in this paper, the *Pbnm* setting is chosen). The real structure can be viewed as a highly distorted cubic perovskite structure with a quadrupled tetragonal unit cell ($a_p\sqrt{2}, a_p\sqrt{2}, 2a_p$) where a_p is the lattice parameter of the cubic perovskite structure (a_0=3.95 Å was used in the present paper also for the tetragonal structure). For orthorhombic structure calculations we used the structural parameters from a neutron diffraction study.[23]

Several calculations[4,5,12,32–35] on the tetragonal phase (i.e., four formula units without the structural distortion) have

shown that LaMnO$_3$ is metallic in all magnetic states and the ground state is FM. This contradicts the experimental data, for both the energy gap [LaMnO$_3$ is believed to be a spin-controlled Mott-Hubbard insulator with the lowest-energy d-d transitions around 2 eV (Ref. 31)] and magnetic AAF ordering in the ground state below 140 K. Our results of cubic LaMnO$_3$ calculations with the primitive cell explain this fact: the tetragonal structure remains in fact cubic, with the tetragonal supercell; since in the primitive unit cell the FM configuration corresponds to the metallic ground state, the same is true for the undistorted tetragonal structure.

However, when the orthorhombic atomic distortions are taken into account, the AAF structure turns out to be the ground state, in agreement with experiment. This is seen from results of both previous and present calculations given in Table II where the relative energies of different magnetic phases are presented (the energy for FM phase is taken as zero energy). Magnetic moments μ on Mn atom and magnetic coupling constants J_{ab} and J_c are also presented there.

We used the Ising model Hamiltonian

$$H = -J_{ab}\sum_{ij} S_{zi}S_{zj} - J_c\sum_{kl} S_{zk}S_{zl}, \qquad (1)$$

where J_{ab} and J_c are exchange integrals (*magnetic coupling constants*) between nearest neighbors in the basal plane (xy)

and between nearest neighbors along the c axis, respectively, S_{zi} stands for the z component of total spin on the magnetic center i, and (ij) and (kl) indicate summation over intraplane and interplane nearest magnetic centers, respectively. Due to possible choice of the Ising Hamiltonian presentation, we stress that Eq. (1) gives positive values for J_{ab} and negative for J_c and contains double summation over each pair of centers. The latter must be taken into account in a comparison with the experimental data. In particular, experimental J_{ab} and J_c values[30] have to be multiplied by a factor of 2. We used a set of equations relating the energy differences for the FM, AAF, GAF, and CAF configurations with the magnetic coupling constants sought for:

$$E(\text{FM}) - E(\text{AAF}) = E(\text{CAF}) - E(\text{GAF}) = -32J_c, \quad (2)$$

$$E(\text{FM}) - E(\text{CAF}) = E(\text{AAF}) - E(\text{GAF}) = -64J_{ab}. \quad (3)$$

Again, to avoid misunderstanding, we write Eqs. (2) and (3) for a quadruple cell, corresponding to *four* formula units. For calculating the coupling constants we used both Eqs. (2) and (3) and performed an averaging. Unfortunately, $E(\text{CAF})$ is not always presented in the published results.

The calculated magnetic coupling constants are compared with the experimental data in the last two columns of Table II. We added to our results [marked by the index[b]] those published in the literature. Our aim was to demonstrate how the calculated magnetic coupling constants depend on the Hamiltonian choice (LDA, UHF, hybrid) and the BS (LCAO, PW, LAPW). The results obtained can be shortly summarized as follows.

Independently from the BS and Hamiltonian used, all calculations mentioned in Table II correctly reproduce the sign of the experimental exchange integrals and their relative values ($|J_{ab}| > |J_c|$). In all UHF and hybrid (B3LYP, B3PW) calculations the exchange integrals agree better with the experimental data than in DFT calculations. We explain this by the incorporation of the Fock exchange into the hybrid methods. For example, if we fix the AO basis (BS3) and analyze a series of the UHF (pure Fock exchange), Fock-50 (50% of Fock exchange) and B3LYP (20% of Fock exchange included), the coupling constants J_{ab} and J_c in this series are getting closer to the experimental values. The effect of the correlation part is smaller (compare B3LYP and B3PW results for BS5). The lack of Fock exchange in LCAO GGA and GGA-PW calculations leads to overestimated values of both magnetic coupling constants. This overestimate is well observed also in previous LAPW, FLMTO, and LDA+U calculations.[32–36] Therefore, in agreement with the conclusion,[6,16,37] we have demonstrated that when calculating the experimentally observable magnetic coupling constants, the *nonlocal* exchange plays an important role. Such hybrid or UHF calculations are practically possible only for the LCAO BS. Our results confirm the conclusion[37] that the CRYSTAL code is a valuable tool for the study of magnetic properties for open-shell transition-metal compounds.

We calculated also the optical gap for the AAF orthorhombic phase. The B3PW LCAO gives 2.9 eV and 4 eV for the Mn d-d and O2p-Mn d transitions, in good agreement with the experiment,[31] whereas the VASP gap of 0.6 eV is an underestimate typical for the DFT.

III. SURFACE CALCULATIONS

A. (001) surface

Periodic first-principles calculations of the crystalline surfaces are usually performed considering a crystal as a stack of planes perpendicular to the surface and cutting out a two-dimensional (2D) slab of finite thickness but periodic in the xy plane. In CRYSTAL-2003 (B3PW LCAO) calculations such a *single slab* is treated indeed, whereas plane-wave calculations, in particular those performed using the VASP code, require translational symmetry along the z axis (repeating slab model). In VASP GGA-PW calculations we used a large vacuum gap of 15.8 Å between periodically repeated slabs.

In fuel cell applications with the operational temperature as high as 800–900 K LaMnO$_3$ stable phase is cubic,[31] and thus Jahn-Teller lattice deformation around Mn ions and the related magnetic and orbital orderings no longer take place. Instead, the main focus here is on the optimal positions for O adsorption and its migration and reaction on the surface. Since the surface relaxation energies are, as we show below, significantly larger than the Jahn-Teller energies (<0.4 eV per Mn ion[31]) and much larger than magnetic exchange energies, the use of the slabs built from the cubic unit cells seems to be justified. To check this point, we performed test calculations for the stoichiometric (001) slabs built both of the orthorhombic and cubic unit cells. The surface energies were calculated following Refs. 13 and 15. For relaxed slabs the reference bulk unit cell energies were taken for the relaxed cubic cells. The (001) surface is polar; this is why we used dipole moment correction option incorporated into the

TABLE III. The calculated surface energies for the unrelaxed and relaxed (E_{su}, E_s) (001) surface energies [in eV per surface square $(a_0)^2$] for LaMnO$_3$ stoichiometric slabs of different thickness. The experimental bulk lattice constant of $a_0 = 3.95$ Å is used. The VASP parameters are *k-point mesh* Monkhorst-Pack $5 \times 5 \times 1$; vacuum gap 15.8 Å, $E_{cut} = 400$ eV. The results of CRYSTAL calculations (k points 4×4) are given in brackets.

N of planes	Slab	E_{su}	E_s
4	NM	1.73 (1.78)	0.94 (0.49)
4	AAF	1.68	0.74
4	FM	1.65 (1.81)	0.77 (0.47)
6	NM	1.74	0.88
8	NM	1.74	0.80
8	AAF	1.74	0.84
8	FM	1.68 (1.43)	0.84
10	NM	1.74	0.72
12	NM	1.74	0.63
12	AAF	1.78	0.89
12	FM	1.69 (0.94)	0.86
14	NM	1.74	0.54

(a)

(b)
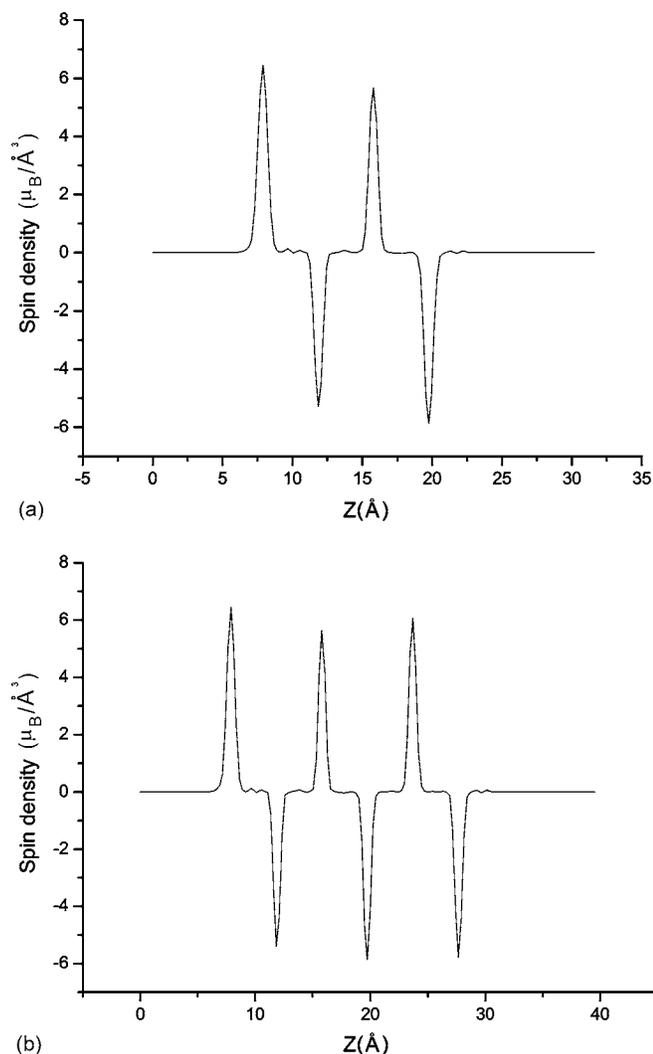
FIG. 1. VASP-calculated spin density along the [001] direction four- (a) and six- (b) layer AAF slabs.

TABLE IV. The VASP atomic relaxation for AAF and FM configurations of a stoichiometric 12-plane slab (displacements are along the z axis, in percent of the bulk lattice constant of 3.95 Å). A positive sign mean outward displacements from the slab center, whereas a negative sign stands for the displacement towards the slab center. O(2) denotes two oxygen atoms in the plane.

Plane	Atom	AAF	FM
1	Mn	0.36	0.53
	O(2)	−4.41	−4.06
2	La	7.83	7.93
	O	−4.03	−2.90
3	Mn	−1.07	−0.41
	O(2)	−5.16	−4.04
4	La	4.32	4.76
	O	−1.72	−0.70
5	Mn	−0.11	−0.04
	O(2)	−2.47	−2.29
6	La	4.96	4.46
	O	0.09	−0.30
7	Mn	−0.68	−0.39
	O(2)	1.22	1.39
8	La	−5.32	−4.81
	O	−0.58	0.09
9	Mn	−0.60	−0.19
	O(2)	1.33	1.43
10	La	−6.02	−5.91
	O	0.69	0.67
11	Mn	0.31	0.79
	O(2)	1.11	1.74
12	La	−9.83	−9.00
	O	1.25	2.19

VASP code.

Keeping in mind the fuel cell applications where surface Mn atoms are supposed to play an essential role, we treated first the *orthorhombic* cells with Mn-terminated stoichiometric slabs consisting of 8 planes and 20 atoms per cell ($Mn_2/O_2\cdots La_2O_2/O_2$). In this structure two O atoms in the upper plane are lower by 0.3 Å than two top Mn atoms. In CRYSTAL calculations for AAF configuration with the rich k set 8×8 we obtained the unrelaxed surface energy to be 4.5 eV per surface unit $[(a_0)^2]$. As the second step, we calculated the surface energies for a similar unrelaxed slab built from cubic unit cells. This slab consists of four planes ($MnO_2/LaO/MnO_2/LaO$). We used the experimental lattice constant for in-plane and interplane distances. The relevant energy of 4.3 eV is smaller than that for the orthorhombic slab. Based on these results, we performed further calculations in this paper for slabs built from *cubic* cells in different magnetic states, varying the slab thickness from 4 to 14 planes. Since slab calculations for rich k-mesh sets are time consuming, in general, and density matrix convergence during solution of Kohn-Sham or Hartree-Fock (in the CRYSTAL

code) self-consistent equations, in particular, is very slow, we used hereafter reduced k-mesh sets as indicated in the tables and performed CRYSTAL optimization only for several distinctive cases.

The results for unrelaxed and relaxed surface energies obtained by both methods for cubic-based slabs of different thickness and three magnetic states are presented in Table III. In the NM configuration spins on Mn atoms are neglected, whereas FM corresponds to all Mn ion spins in a parallel orientation, and in AAF configuration Mn ion spins are parallel in the x, y plane but antiparallel along the z direction, respectively. The surface energy for the unrelaxed surface (the *cleavage energy*) obtained in the VASP calculations slightly depends on the slab thickness and the magnetic state; in CRYSTAL calculations the cleavage energy depends much stronger on the slab thickness. The relaxed surface energy E_s calculated by both methods considerably depends on the slab thickness. The lattice relaxation reduces the surface energy by about a factor of 2, down to a surprisingly low value of 0.86 eV for the FM and 0.89 eV for the AAF magnetic configuration of the 12-plane slab. As we show below, this value is lower than that for the (110) surface energy. This means
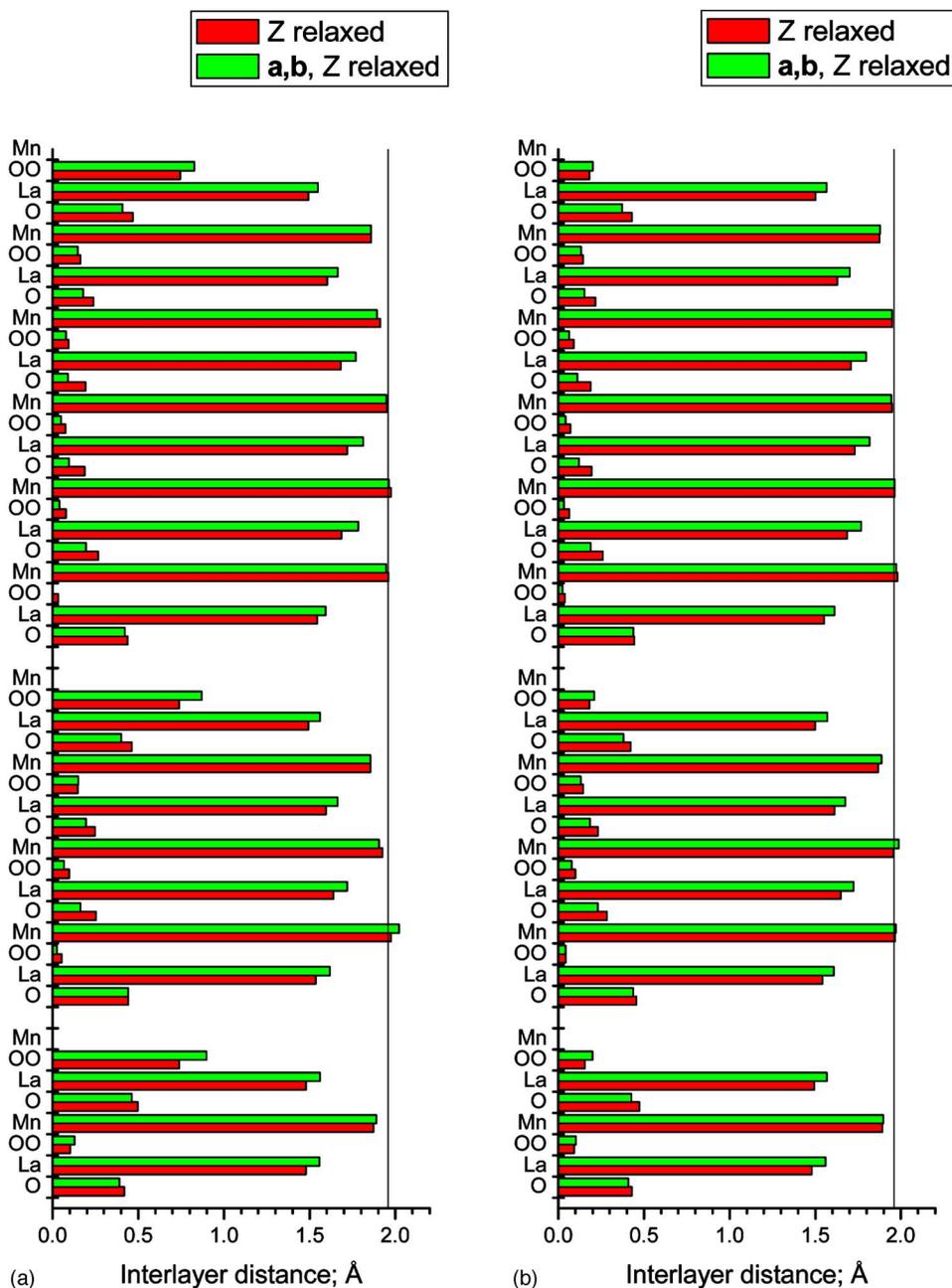
FIG. 2. (Color online) The VASP-calculated for (001) surface interatomic distances along the z axis in the relaxed AAF (a) and FM (b) slabs containing 4, 8, and 12 planes. The distance between the planes in the bulk is shown by the vertical solid black line.

that the (001) surface is energetically more favorable and thus MnO_2 termination could play an important role in the surface reactivity (unless entropy effects change this result).

Several general conclusions could be also drawn from our calculations. (i) B3PW LCAO calculations are in good agreement with the VASP calculations for the cleavage energies (1.43 eV, which is higher than those obtained earlier in HF calculations[13]), but yield typically lower relaxed surface energies (0.47 eV for the FM four-plane slab; we compare below the VASP- and CRYSTAL-calculated surface relaxation). (ii) The calculated total magnetic moment is nonzero for the AAF slabs; this is $0.9\mu_B$, $0.65\mu_B$, and $1.46\mu_B$ for the 4-, 8-, and 12-plane slabs, respectively. This is caused by different magnetic moments on Mn atoms occupying different positions in the asymmetric $MnO_2 \cdots LaO$ slab, as illustrated in Fig. 1.

The relative atomic displacements are presented in Table IV. The atomic displacements for the AAF and FM magnetic configurations are close but strongly differ from those in (not shown here) the NM configuration. All Mn atoms are very moderately displaced from the perfect lattice sites ($<1\% a_0$), even on the Mn-terminated surface. Unlike Mn, La ions are strongly displaced towards the nearest (outermost) MnO_2 planes. O ions are strongly displaced inwards on the Mn-terminated surface but slightly move outwards on the La-terminated surface. Both MnO_2 and LaO terminations demonstrate large (5%–10%) *rumpling* (relative displacement of Me (=La, Mn) and O ions from the crystallographic MeO plane). Large La displacements even in the central planes indicate that probably our slab is still relatively thin and polarized. Moreover, La and O displacements on the slab bottom have opposite sign with similar displacements in the

TABLE V. CRYSTAL- and VASP-calculated effective charges Q of atoms in the LaMnO$_3$ bulk cubic crystals (in e) (a) and the charges of the eight-plane AAF and FM slabs, as well as their difference ΔQ with respect to the bulk values in the cubic (tetragonal) unit cell (b). Numbers in brackets are given for the unrelaxed surface.

Atoms	CRYSTAL-NM	CRYSTAL-FM	VASP-FM, AAF
(a)			
La	2.61	2.62	2.13
Mn	1.87	2.04	1.85
O	−1.49	−1.55	−1.29

		VASP							CRYSTAL	
		FM				AAF			FM	
Plane	Atom	Q		ΔQ		Q		ΔQ		Q	ΔQ
(b)											
1	Mn	(1.86)	1.66	(0.01)	−0.19	(1.85)	1.60	(0.01)	−0.25	(2.05)	(0.01)
	O(2)	(−1.15)	−1.21	(0.14)	0.08	(−1.15)	−1.22	(0.14)	0.07	(−1.33)	(0.22)
2	La	(2.00)	2.07	(−0.13)	−0.06	(2.00)	2.06	(−0.13)	−0.07	(2.57)	(−0.05)
	O	(−1.18)	−1.24	(0.11)	0.05	(−1.18)	−1.19	(0.11)	0.10	(−1.48)	(0.07)
3	Mn	(1.87)	1.81	(0.03)	−0.04	(1.87)	1.77	(0.02)	−0.08	(2.02)	(−0.02)
	O(2)	(−1.30)	−1.24	(−0.01)	0.05	(−1.30)	−1.26	(−0.01)	0.03	(−1.50)	(0.05)
4	La	(2.03)	2.06	(−0.10)	−0.07	(2.03)	2.09	(−0.10)	−0.04	(2.60)	(−0.02)
	O	(−1.19)	−1.24	(0.10)	0.05	(−1.18)	−1.17	(0.11)	0.12	(−1.52)	(0.03)
5	Mn	(1.72)	1.69	(−0.13)	−0.15	(1.73)	1.71	(−0.11)	−0.13	(2.01)	(−0.03)
	O(2)	(−1.35)	−1.28	(−0.06)	0.01	(−1.36)	−1.27	(−0.07)	0.03	(−1.58)	(−0.02)
6	La	(2.02)	2.06	(−0.11)	−0.07	(2.02)	2.02	(−0.11)	−0.10	(2.60)	(−0.01)
	O	(−1.20)	−1.24	(0.09)	0.05	(−1.20)	−1.25	(0.09)	0.04	(−1.51)	(0.04)
7	Mn	(1.83)	1.84	(−0.01)	−0.01	(1.85)	1.82	(0.00)	−0.03	(1.97)	(−0.07)
	O(2)	(−1.30)	−1.32	(−0.01)	−0.03	(−1.31)	−1.31	(−0.02)	−0.02	(−1.58)	(−0.02)
8	La	(1.77)	1.99	(−0.36)	−0.14	(1.76)	1.98	(−0.37)	−0.15	(2.44)	(−0.17)
	O	(−1.32)	−1.35	(−0.03)	−0.06	(−1.32)	−1.33	(−0.03)	−0.04	(−1.77)	(−0.22)

LaO plane second from the slab top. Unlike AAF and FM, most of the ions in NM slab are displaced strongly inwards, which means a strong compression of the slab. This results directly from the fact that the VASP-optimized NM bulk lattice constant (3.83 Å) is much smaller than the experimental value of a_0.

In Fig. 2 we illustrate how the interatomic distances change after relaxation of three slabs consisting of 4, 8, and 12 planes. In the 12-plane slab most of the interplane distances are close to those in the bulk (except for two surface planes for both terminations which are strongly disturbed). In contrast, in the smallest 4-plane slab all planes are disturbed and their arrangement is similar to those in thicker slabs. Comparison of the FM and AAF configurations [Figs. 2(a) and 2(b)] demonstrates their similarity except for the surface rumpling on the MnO$_2$-terminated surface. This is much larger for the AAF as compared to the FM (where rumpling is quite small).

In order to characterize the electronic density distribution, the Bader charges[38] were obtained in the VASP calculations and compared with the Mulliken charges in CRYSTAL calculations (Table V). Note that for both methods the cubic bulk charge values [Table V(a)] are considerably smaller than the

relevant formal charges of $3e$, $3e$, and $-2e$ on La, Mn, and O atoms, respectively. This is caused by the covalent contribution to the chemical bonding between Mn and O ions in the bulk. The following important conclusion could be drawn from Table V(b): the effective charges are similar for different magnetic configurations but strongly depend on the surface relaxation. This should affect also the surface magnetic moments on Mn atoms. However, both Mn and O charges on the relaxed MnO$_2$ surface are considerably smaller (both ions are closer to neutral Mn and O atoms), which decreases partly the dipole moment of a slab. This very likely results from an increased covalent contribution to Mn—O bonding on the surface, in line with our recent observation for the SrTiO$_3$ surface.[15] In contrast, both La and O on the surface attract considerable electron density; i.e., this plane becomes more conductive. We have calculated also the effective charges in the 12-plane slab and found that those in the slab center (planes 5 and 6) are very close to the bulk values which indicates that such a slab is thick enough for the surface effect to decay. In Fig. 3 the difference between the electronic density around Mn, La, and O ions on unrelaxed surface and similar density in the bulk crystal is plotted. In agreement with Table V(b), one can see that before relax-
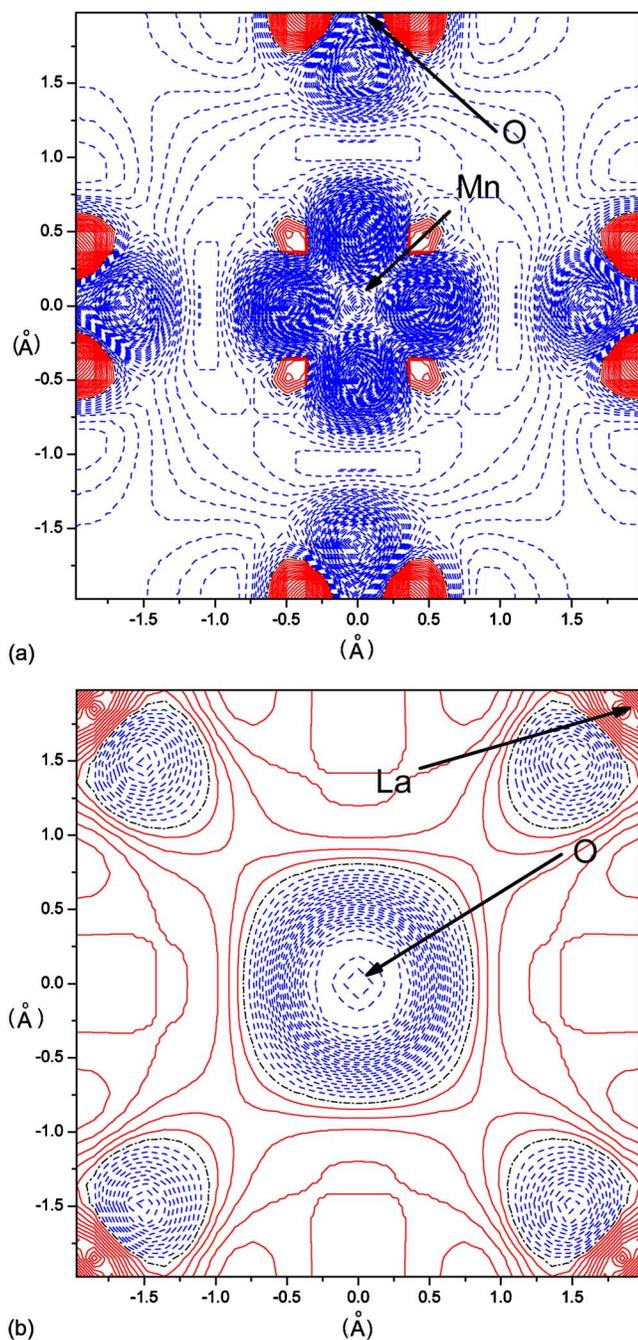
(a)

(b)

FIG. 3. (Color online) The VASP-calculated difference of electron density maps for the top unrelaxed MnO_2 (a) and LaO (b) planes with respect to self-consistent density in the bulk. Solid (red) and dashed (blue) lines denote the excess and deficiency of the electron density; the isodensity increment is $0.01e/Å^3$.

ation La ions on the LaO-terminated surface attracts additional electron density, even more than in relaxed case, while O ions remain similar to the bulk. In contrast, on the MnO_2-terminated surface Mn ions are close to the bulk but O ions become more positive.

In order to compare with the VASP results, Table V presents also the CRYSTAL calculations for the effective charges in the $LaMnO_3$ bulk and in an eight-plane unrelaxed stoichiometric slab in the FM configurations. (Similar results

for the HF calculations were discussed in Ref. 13.) In all cases, B3PW and UHF (cited in Table V) give larger effective (Mulliken) charges. Changes of the effective charges with respect to the bulk are qualitatively similar to those discussed for VASP. In both methods, surface La and O ions attract additional electron density, which makes this plane more metallic, as compared to similar plane in the bulk (in agreement with the HF results[13]). These conclusions are true for all three magnetic configurations treated in the CRYSTAL calculations.

Along with the calculations for asymmetric $MnO_2\cdots LaO$ stoichiometric slabs which reveal dipole moment perpendicular to the surface, we calculated also two types of *symmetric* slabs—$MnO_2/LaO\cdots MnO_2$ and LaO/$MnO_2\cdots LaO$—consisting of seven planes and having by symmetry no dipole moments. The calculated average surface energies[13] in the FM state are as follows: in the case of the unrelaxed surfaces 2.60 eV and 2.06 eV for VASP and CRYSTAL and 1.69 eV and 0.87 eV in the case of the relaxed surfaces, respectively. The CRYSTAL energies are smaller, especially for the relaxed surface. Both methods give higher seven-plane slab energies than for the eight-plane slabs, likely due to the nonstoichiometry of the former slabs.

In Table VI we compare the atomic displacements and effective charges for the seven-plane FM slabs calculated using both VASP and CRYSTAL codes. The directions of atomic displacements are similar in most cases but the magnitudes differ. If we compare VASP results with those for the eight-plane slab (Table IV), directions of atomic displacements for both terminations, MnO_2 and LaO, are the same but the magnitudes also differ, which indicates probably that these slabs are not thick enough. This is in contrast with similar calculations for the isostructural $SrTiO_3$ (Ref. 15) where atomic relaxation is marginal already in the third near-surface plane whereas seven- and eight-plane slabs give close results. The LaO-terminated surface is considerably more conductive in both methods, VASP and CRYSTAL.

B. (110) surface

We calculated also the atomic and electronic structure of the (110) $LaMnO_3$ surface in the FM configuration. Similarly to the (001) surface, we modeled both the eight-plane stoichiometric asymmetrical slabs $O_2/LaMnO/\cdots O_2$ and two types of seven-plane nonstoichiometric symmetric slabs without dipole moments ($O_2/LaMnO\cdots O_2$ and LaMnO/$O_2\cdots LaMnO$). As follows from Table VII, in all three cases the (110) surface energy is larger than that for the above discussed (001) surface. (We came to the same conclusion in the HF calculations.[13]) Second, the VASP-calculated cleavage energies for seven- and eight-plane slabs practically coincide. This shows that the dipole moments play no essential role here. In addition, CRYSTAL calculations again demonstrate larger surface relaxation energy than those performed by VASP: starting with considerably larger cleavage energy, CRYSTAL calculations end up with a smaller relaxed surface energy.

We compare the relevant atomic relaxation and the effective charges obtained by both methods in Table VIII. Unlike

TABLE VI. Atomic displacements Δz along the z axis (in percent of the bulk lattice constant), the effective charges (in e), and their deviation form the bulk values calculated for the two seven-plane (001) FM slabs with MnO_2 (a) and LaO (b) terminations. Due to a slab symmetry, the first four planes are given only.

		VASP			CRYSTAL		
Plane	Atom	Δz	Q	ΔQ	Δz	Q	ΔQ
(a)							
1	Mn	1.68	1.67	−0.17	−0.58	1.98	−0.07
	O(2)	−2.98	−1.19	0.11	−4.16	−1.41	0.14
2	La	6.08	2.08	−0.05	4.44	2.56	−0.06
	O	−1.80	−1.16	0.14	−2.63	−1.46	0.10
3	Mn	0.57	1.71	−0.14	−0.66	2.05	0.00
	O(2)	−1.73	−1.15	0.15	−2.81	−1.44	0.11
4	La	0.00	2.00	−0.13	0.00	2.59	−0.03
	O	0.00	−1.19	0.11	0.00	−1.44	0.11

		VASP			CRYSTAL		
Plane	Atom	Δz	Q	ΔQ	Δz	Q	ΔQ
(b)							
1	La	−6.86	1.96	−0.17	−5.71	2.53	−0.08
	O	4.51	−1.33	−0.03	7.08	−1.71	−0.16
2	Mn	2.02	1.50	−0.34	1.7	1.87	−0.17
	O(2)	1.89	−1.23	0.07	2.05	−1.62	−0.07
3	La	−2.07	2.02	−0.11	−1.37	2.60	−0.02
	O	0.96	−1.21	0.09	−0.82	−1.56	−0.01
4	Mn	0.00	1.50	−0.35	0.00	2.05	0.00
	O(2)	0.00	−1.24	0.06	0.00	−1.52	0.04

the (001) surface, now atoms in O_2 planes experience also in-plane displacements along the y axis. Eight-plane slabs in both methods show large surface La displacements inwards the slab center (6%–7% a_0), whereas Mn and O ions move in the opposite direction. As a result, this surface exhibits very large rumpling. Both methods agree in that the LaMnO-terminated surface is strongly negatively charged with respect to the bulk. There is also good agreement on the considerable inward relaxation of ions on the O terminated surface (2.5%–3% a_0) which is positively charged with respect to the bulk.

TABLE VII. Calculated surface energies for the unrelaxed and relaxed (E_{su}, E_s) surface energies (in eV) for the (110) FM slabs of eight and seven planes. Parameters are (in VASP calculations): *k-point mesh* Monkhorst-Pack $4 \times 3 \times 2$; the vacuum gap 22.07 Å, $E_{cut} = 400$ eV. For a comparison with the (001) surface, surface energies are given for the same square unit a_0^2.

No. of planes	Method	E_{su}	E_s
8	GGA-PW	2.59	1.29
8	B3PW	4.05	0.95
7	GGA-PW	2.60	1.69

Calculations for the symmetric slabs without dipole moments (*b* and *c*) reveal similar displacements on the LaMnO-terminated plane and even larger negative charge of this surface; in particular, the Mn ion get extra 0.8e as compared to the bulk. Note that O charges inside slab are close to those in the bulk. On the contrary, the O_2-terminated surface reveals positive charge in both methods, whereas charges of deeper planes are close to those in the bulk crystal.

IV. CONCLUSIONS

Our results, in line with the study,[6] demonstrate that it is a combination of the *nonlocal exchange* with correlation effects realized in the hybrid functionals which considerably narrows the gap between calculated and experimental magnetic coupling constants. This questions the generally accepted idea that DFT is better suited than UHF and related methods for the study of manganites, in particular, $LaMnO_3$.

Results of our B3PW LCAO and GGA-PW calculations for the $LaMnO_3$ surfaces show reasonable agreement for atomic displacements, effective charges, and surface energies. The effective charges of surface atoms considerably depend on the surface relaxation and less on the particular (FM or AAF) magnetic configuration. Our findings confirm our previous HF-based conclusion[13] that the polar (001) sur-

TABLE VIII. The effective charges Q (in e), their deviations from those in the bulk (ΔQ), and displacements (in percent of $a_0\sqrt{2}$) along the y and z axes for the eight-plane (110) slab (a) as well as for seven-plane LaMnO- (b) and O_2- (c) terminated slabs in the FM state.

Plane	Atom	VASP				CRYSTAL			
		Δy	Δz	Q	ΔQ	Δy	Δz	Q	ΔQ
(a)									
1	La	0.00	−6.10	1.87	−0.25	0.00	−7.28	2.46	−0.16
	Mn	0.00	3.40	1.25	−0.59	0.00	2.9	1.78	−0.27
	O	0.00	6.61	−1.30	0.00	0.00	12.37	−1.75	−0.19
2	O(2)	−1.45	3.26	−1.30	0.00	−1.60	3.97	−1.70	−0.15
3	La	0.00	−4.77	2.01	−0.12	0.00	−5.64	2.54	−0.07
	Mn	0.00	−0.17	1.65	−0.20	0.00	−1.75	1.91	−0.13
	O	0.00	1.13	−1.22	0.08	0.00	0.33	−1.60	−0.04
4	O(2)	−1.23	1.67	−1.24	0.06	−1.99	−0.19	−1.52	0.03
5	La	0.00	5.20	2.02	−0.11	0.00	5.47	2.55	−0.06
	Mn	0.00	1.62	1.72	−0.13	0.00	1.9	2.06	0.02
	O	0.00	−1.56	−1.17	0.13	0.00	−0.19	−1.46	0.09
6	O(2)	−1.53	−1.64	−1.20	0.10	−0.91	−1.14	−1.47	0.08
7	La	0.00	11.17	2.14	0.01	0.00	7.85	2.56	−0.06
	Mn	0.00	3.31	1.78	−0.06	0.00	3.87	2.07	0.03
	O	0.00	−1.55	−1.10	0.20	0.00	−1.41	−1.41	0.14
8	O(2)	−1.32	−2.48	−1.06	0.24	−0.93	−3.36	−1.17	0.39

Plane	Atom	VASP			
		Δy	Δz	Q	ΔQ
(b)					
1	La	0.00	−6.43	1.72	−0.41
	Mn	0.00	3.36	1.04	−0.80
	O	0.00	1.98	−1.25	0.05
2	O(2)	−0.34	0.25	−1.30	0.00
3	La	0.00	−0.47	2.06	−0.07
	Mn	0.00	−0.43	1.57	−0.28
	O	0.00	−0.31	−1.27	0.03
4	O(2)	0.00	0.00	−1.26	0.04

Plane	Atom	VASP				CRYSTAL			
		Δy	Δz	Q	ΔQ	Δy	Δz	Q	ΔQ
(c)									
1	O(2)	1.02	−4.98	−0.94	0.36	−0.59	−8.15	−1.11	0.45
2	La	0.00	2.56	2.15	0.02	0.00	1.76	2.57	−0.05
	Mn	−0.01	2.15	1.77	−0.08	0.00	−0.79	2.12	0.07
	O	0.00	−3.49	−1.11	0.19	0.00	−6.46	−1.36	0.20
3	O(2)	0.22	−1.50	−1.16	0.14	−0.47	−0.61	−1.42	0.13
4	La	0.00	0.00	2.13	0.00	0.00	0.00	2.58	−0.04
	Mn	0.01	0.00	1.79	−0.06	0.00	0.00	2.34	0.29
	O(2)	0.00	0.00	−1.19	0.11	0.00	0.00	−1.47	0.09

face has a lower energy than the (110) one. This conclusion is important for the modeling of surface adsorption and LaMnO$_3$ reactivity, which is now in progress. The surface relaxation energy is typically of the order of $1-1.5$ eV (per square unit a_0^2)—i.e., much larger than the tiny difference between various magnetic structures. Moreover, the calculated surface energy for the slab built from orthorhombic unit cells is close and even slightly larger than that for the cubic unit cells. These two facts justify the use in surface and adsorption modeling of slabs built from the cubic cells. This is a very important observation since the detailed adsorption and migration modeling—e.g., for surface O atoms at moderate coverages which is relevant for fuel cell applications—is very time consuming even for the smallest slab thicknesses.

[1] J. Fleig, K. D. Kreuer, and J. Maier, *Handbook of Advanced Ceramics* (Elsevier, Singapore, 2003), p. 57.

[2] G. Banach and W. M. Temmerman, Phys. Rev. B **69**, 054427 (2004); H. Zenia, G. A. Gehring, G. Banach, and W. M. Temmerman, Phys. Rev. B **71**, 024416 (2005).

[3] A. Filipetti and W. E. Pickett, Phys. Rev. Lett. **83**, 4184 (1999); Phys. Rev. B **62**, 11571 (2000).

[4] Y.-S. Su, T. A. Kaplan, S. D. Mahanti, and J. F. Harrison, Phys. Rev. B **61**, 1324 (2000).

[5] M. Nicastro and C. H. Patterson, Phys. Rev. B **65**, 205111 (2002).

[6] D. Munoz, N. M. Harrison, and F. Illas, Phys. Rev. B **69**, 085115 (2004).

[7] G. Trimarchi and N. Binggeli, Phys. Rev. B **71**, 035101 (2005).

[8] P. Pavindra, A. Kjekshus, H. Fjellvag, A. Delin, and O. Eriksson, Phys. Rev. B **65**, 064445 (2002).

[9] E. A. Kotomin, E. Heifets, J. Maier, and W. A. Goddard III, Phys. Chem. Chem. Phys. **5**, 4180 (2003).

[10] E. Heifets, R. A. Evarestov, E. A. Kotomin, S. Dorfman, and J. Maier, Sens. Actuators B **100**, 81 (2004).

[11] E. A. Kotomin, E. Heifets, S. Dorfman, D. Fuks, A. Gordon, and J. Maier, Surf. Sci. **566**, 231 (2004).

[12] R. A. Evarestov, E. A. Kotomin, E. Heifets, J. Maier, and G. Borstel, Solid State Commun. **127**, 367 (2003).

[13] R. A. Evarestov, E. A. Kotomin, D. Fuks, J. Felsteiner, and J. Maier, Appl. Surf. Sci. **238**, 457 (2004).

[14] E. A. Kotomin, R. A. Evarestov, Yu. A. Mastrikov, and J. Maier, Phys. Chem. Chem. Phys. **7**, 2346 (2005).

[15] S. Piskunov, E. A. Kotomin, E. Heifets, J. Maier, R. I. Eglitis, and G. Borstel, Surf. Sci. **575**, 75 (2005); X. Feng, Phys. Rev. B **69**, 155107 (2004).

[16] F. Cora, M. Alfredsson, G. Mallia, D. Middleniss, W. C. Mackrodt, R. Dovesi, and R. Orlando, Struct. Bonding (Berlin) **113**, 171 (2004).

[17] V. R. Saunders, R. Dovesi, C. Roetti, R. Orlando, C. M. Zicovich-Wilson, N. M. Harrison, K. Doll, B. Civalleri, I. J. Bush, Ph. D'Arco, and M. Llunell, CRYSTAL-2003 User's Manual, 2003.

[18] G. Kresse and J. Furthmüller, VASP the Guide, University of Vienna, Austria, 2003.

[19] A. Becke, J. Chem. Phys. **98**, 5648 (1993).

[20] J. P. Perdew and Y. Wang, Phys. Rev. B **33**, 8800 (1986); **40**, 3399 (1989); **45**, 13244 (1992); J. Perdew, *Electronic Structure of Solids* (Akademie Verlag, Berlin, 1991).

[21] S. Piskunov, E. Heifets, R. I. Eglitis, and G. Borstel, Comput. Mater. Sci. **29**, 165 (2004).

[22] C. Lee, W. Yang, and R. G. Parr, Phys. Rev. B **37**, 785 (1988).

[23] J. Rodríguez-Carvajal, M. Hennion, F. Moussa, A. H. Moudden, L. Pinsard, and A. Revcolevschi, Phys. Rev. B **57**, R3189 (1998).

[24] http://www.chimifm.unito.it/teorica/crystal/basis_sets/mendel.html

[25] P. J. Hay and W. R. Wadt, J. Chem. Phys. **82**, 270 (1984); **82**, 284 (1984); **82**, 299 (1984).

[26] F. Freyria Fava, Ph. D. Arco, R. Orlando, and R. Dovesi, J. Phys.: Condens. Matter **9**, 489 (1997).

[27] M. D. Towler, N. Allan, N. M. Harrison, V. R. Saunders, W. C. Mackrodt, and E. Apra, Phys. Rev. B **50**, 5041 (1994).

[28] M. Dolg, H. Stall, A. Savin, and H. Preuss, Theor. Chim. Acta **75**, 173 (1989).

[29] J. K. Perry, J. Tahir-Kheli, and W. A. Goddard III, Phys. Rev. B **63**, 144510 (2001).

[30] F. Moussa, M. Hennion, J. Rodriguez-Carvajal, H. Moudden, L. Pinsard, and A. Revcolevschi, Phys. Rev. B **54**, 15149 (1996).

[31] N. N. Kovaleva, A. V. Boris, C. Bernhard, A. Kulakov, A. Pimenov, A. M. Balbashov, G. Khaliullin, and B. Keimer, Phys. Rev. Lett. **93**, 147204 (2004).

[32] N. Hamada, H. Sawada, I. Solovyev, and K. Terakura, Physica B **237–238**, 11 (1997).

[33] P. Ravindran, A. Kjekshus, H. Fjellvag, A. Delin, and O. Eriksson, Phys. Rev. B **65**, 064445 (2002).

[34] R. Lorenz, R. Hafner, D. Spisak, and J. Hafner, J. Magn. Reson., Ser. A **226–230**, 889 (2001).

[35] W. Y. Hu, M. C. Quian, Q. Q. Zheng, H. Q. Lin, and H. K. Wong, Phys. Rev. B **61**, 1223 (2000).

[36] T. Saitoh, A. E. Boquet, T. Mizokawa, H. Namatame, A. Fujimori, M. Abbate, Y. Takeda, and M. Takano, Phys. Rev. B **51**, 13942 (1995).

[37] E. Ruiz, M. Llunell, and P. Alemany, J. Solid State Chem. **176**, 400 (2003).

[38] G. Henkelman, A. Arnaldsson, and H. Jónsson, Comput. Mater. Sci. (to be published).